Human DNA Polymerase ν Catalyzes Correct and Incorrect DNA Synthesis with High Catalytic Efficiency*

A. S. Prakasha Gowda, George-Lucian Moldovan, and ⓘ Thomas E. Spratt[1]

From the Department of Biochemistry and Molecular Biology, Milton S. Hershey Medical Center, Pennsylvania State University College of Medicine, Hershey, Pennsylvania 17033

Background: DNA polymerase ν is a low fidelity polymerase with an unknown function.
Results: The kinetic mechanism of correct and incorrect base pair formation was determined.
Conclusion: Phosphodiester bond formation is rapid for both correct and mispair formation.
Significance: The presence of a mispair does not induce the polymerase to adopt a low catalytic conformation.

DNA polymerase ν (pol ν) is a low fidelity A-family polymerase with a putative role in interstrand cross-link repair and homologous recombination. We carried out pre-steady-state kinetic analysis to elucidate the kinetic mechanism of this enzyme. We found that the mechanism consists of seven steps, similar that of other A-family polymerases. pol ν binds to DNA with a K_d for DNA of 9.2 nM, with an off-rate constant of 0.013 s^{-1} and an on-rate constant of 14 μM^{-1} s^{-1}. dNTP binding is rapid with K_d values of 20 and 476 μM for the correct and incorrect dNTP, respectively. Pyrophosphorylation occurs with a K_d value for PP$_i$ of 3.7 mM and a maximal rate constant of 11 s^{-1}. Pre-steady-state kinetics, examination of the elemental effect using dNTPαS, and pulse-chase experiments indicate that a rapid phosphodiester bond formation step is flanked by slow conformational changes for both correct and incorrect base pair formation. These experiments in combination with computer simulations indicate that the first conformational change occurs with rate constants of 75 and 20 s^{-1}; rapid phosphodiester bond formation occurs with a K_{eq} of 2.2 and 1.7, and the second conformational change occurs with rate constants of 2.1 and 0.5 s^{-1}, for correct and incorrect base pair formation, respectively. The presence of a mispair does not induce the polymerase to adopt a low catalytic conformation. pol ν catalyzes both correct and mispair formation with high catalytic efficiency.

DNA polymerase ν (pol[2] ν) is one of the 17 DNA polymerases encoded by the human genome (1). Although the roles of many of these polymerases are known (2–4), the function of pol ν has yet to be elucidated. There is evidence that pol ν functions in cross-link repair and/or homologous recombination. For instance, mutations in *mus308*, the *Drosophila* ortholog of pol ν, cause hypersensitivity to cross-linking agents (nitrogen mustard and cisplatin) but not methyl methanesulfonate (5, 6). In human cells, siRNA knockdown of pol ν also causes sensitivity to cross-linking agents and impairs homologous recombination (7, 8). Consistent with a direct role in the repair of these cross-linking agents, pol ν can bypass a psoralen-DNA intrastrand cross-link and DNA-DNA cross-links with linkages in the major groove of the DNA (8, 9).

DNA polymerases have been categorized into families based upon sequence homology. pol ν as well as pols γ and θ are human A-family polymerases. Other members of this family that have been extensively studied are DNA polymerase I of *Escherichia coli* (Klenow fragment, KF) (10–13), *Thermus aquaticus* (Taq pol) (14, 15), *Bacillus stearothermophilus* (*BF*) (16, 17), and bacteriophage T7 (T7 pol) (18, 19), as well as pol γ (20–22). Although the A-family polymerases have sequence similarities, differences in sequence provide specialized functions. For instance, *E. coli* pol I is a high fidelity polymerase with a 3'- to 5'-exonuclease proofreading activity as well as a 5'- to 3'-exonuclease activity. These activities let *E. coli* pol I function in Okazaki fragment synthesis as well as DNA repair in *E. coli*. pol γ is a multisubunit protein with high fidelity polymerase, 3'- to 5'-exonuclease proofreading, and 5'-deoxyribose phosphate lyase activities that enable pol γ to be the sole polymerase responsible for the replication, recombination, and repair of mitochondrial DNA (23).

pol ν is a 900-amino acid protein, in which the C-terminal 419 residues are highly related to the polymerase domains of A-family polymerases (1). pol ν lacks the helicase, exonuclease, and lyase activities of other A-family polymerases. It exhibits low fidelity, with base pair substitution and deletion rates similar to Y-family polymerases (24). The polymerase is especially unfaithful with a high frequency for the formation of dG/dT mismatch formation (24, 25). Pre-steady-state analysis showed that the lower fidelity of pol ν compared with that of KF(exo−) is due to lower k_{pol} parameters for correct dNTP incorporation (26).

The complete kinetic profiles of *E. coli* pol I (10–13, 27) and bacteriophage T7 polymerase (18, 19) have been determined. The mechanism consists of seven steps shown in Fig. 1*A*, in which phosphodiester bond formation, step 4, is flanked by conformational changes that are rate-limiting. Upon binding

[1] To whom correspondence should be addressed: Dept. of Biochemistry and Molecular Biology, Pennsylvania State University, H171, 500 University Dr., Hershey, PA 17033-0850. Tel.: 717-531-4623; Fax: 717-531-7072; E-mail: tes13@psu.edu.

[2] The abbreviations used are: pol, polymerase; BF, large fragment of DNA polymerase I of *B. stearothermophilus*; KF, Klenow fragment of DNA polymerase I of *E. coli*; Taq pol, *T. aquaticus* DNA polymerase I; T7, pol, bacteriophage T7 DNA polymerase.
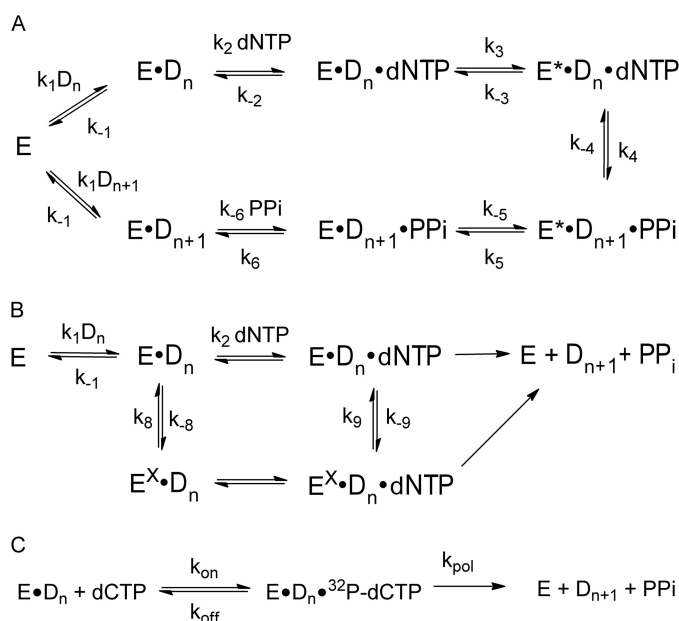
A

$$E \xrightleftharpoons[k_{-1}]{k_1 D_n} E \cdot D_n \xrightleftharpoons[k_{-2}]{k_2\, dNTP} E \cdot D_n \cdot dNTP \xrightleftharpoons[k_{-3}]{k_3} E^* \cdot D_n \cdot dNTP$$

$$\downarrow\, k_4 \uparrow k_{-4}$$

$$E \xrightleftharpoons[k_{-1}]{k_1 D_{n+1}} E \cdot D_{n+1} \xrightleftharpoons[k_6]{k_{-6}\, PPi} E \cdot D_{n+1} \cdot PPi \xrightleftharpoons[k_5]{k_{-5}} E^* \cdot D_{n+1} \cdot PPi$$

B

$$E \xrightleftharpoons[k_{-1}]{k_1 D_n} E \cdot D_n \xrightleftharpoons[]{k_2\, dNTP} E \cdot D_n \cdot dNTP \longrightarrow E + D_{n+1} + PP_i$$

$$k_8 \updownarrow k_{-8} \qquad k_9 \updownarrow k_{-9}$$

$$E^X \cdot D_n \longrightarrow E^X \cdot D_n \cdot dNTP$$

C

$$E \cdot D_n + dCTP \xrightleftharpoons[k_{off}]{k_{on}} E \cdot D_n \cdot {}^{32}P\text{-}dCTP \xrightarrow{k_{pol}} E + D_{n+1} + PPi$$

FIGURE 1. **DNA polymerase mechanisms.** *A,* induced fit mechanism for DNA polymerase ν. *B,* polymerase mechanism with inactive conformations. *C,* mechanism to analyze dNTP pulse-chase experiment.

the correct dNTP, the polymerase is able to form an active conformation that catalyzes phosphodiester bond formation rapidly. When an incorrect dNTP binds, the enzyme is unable to adopt the highly catalytic conformation, and phosphodiester bond formation becomes rate-limiting (11, 12, 18, 28). The kinetic schemes of the low fidelity Dpo4 and pol κ also consist of those seven steps, with the difference that the rate phosphodiester bond formation is similar to those of the conformational changes (29, 30). In this study, we evaluated the kinetic mechanism of pol ν and found that similar to KF and T7 pol, pol ν catalyzes correct base pair formation with a rapid phosphodiester bond formation step. In contrast to its high fidelity cousins, pol ν catalyzes mispair formation via the same mechanism. Despite the binding of the wrong dNTP, the enzyme is able to form a high catalytic conformation.

Experimental Procedures

General—[γ-^{32}P]ATP, [α-^{32}P]dCTP, and [α-^{32}P]dATP were purchased from PerkinElmer Life Sciences, and T4 polynucleotide kinase was from USB®/Affymetrix. The dNTPs (ultrapure grade) were purchased from GE Healthcare, and the concentrations were determined by UV absorbance (31). Oligodeoxynucleotides were synthesized at the Macromolecular Core Facility at the Pennsylvania State University College of Medicine. The sequences of the oligodeoxynucleotides are shown in Table 1. The primer was ^{32}P-labeled with [γ-^{32}P]ATP and annealed with a 20% excess of the template as described previously (32). The P15/T24 substrate was used in all except the pyrophosphorylation experiments and is referred to as the DNA substrate.

pol ν was purified by a modification of the method described by Takata *et al.* (24). The protein has a deletion of a C-terminal polyproline segment, an N-terminal His tag, and C-terminal FLAG tag. After lysing the cells, the resulting supernatant was loaded onto a nickel-nitrilotriacetic acid column (3 ml), and the

TABLE 1
Oligodeoxynucleotide sequences

P15-	5'- G C A C C G C A G A C G C A G	-3'
P16C	5'- G C A C C G C A G A C G C A G C	-5'
P16T	5'- G C A C C G C A G A C G C A G T	-5'
T24	3'- C G T G G C G T C T G C G T C **G** A C A G C G T C -5'

enzyme was eluted with an imidazole gradient. Purity was evaluated by SDS-PAGE, and the protein concentration was determined by the Qubit protein assay kit (Life Technologies, Inc.).

Kinetic Analyses—All assays with pol ν were performed in 40 mM Tris-HCl (pH 8.0), 5 mM MgCl$_2$ at 37 °C. The concentrations reported for each species are those that occurred during the reaction. The reactions were initiated by the addition of dNTP containing MgCl$_2$ to preincubated protein and DNA in buffer. Steady-state reactions were quenched with equal volumes of STOP solution containing 10% 0.5 M Na$_2$EDTA, 90% formamide, and 0.025% (w/v) xylene cyanol and bromphenol blue. Fast reactions were carried out with an RQF-3 quench flow apparatus (KinTek) and were quenched with 0.3 M Na$_2$EDTA, which was diluted with STOP solution to load onto the gel. The progress of the reaction was analyzed by denaturing PAGE, and the radioactivity on the gel was visualized with a Typhoon 9200 Variable Mode Imager (GE Healthcare). The reactions were quantitated by dividing the total radioactivity in the product band(s) by the radioactivity in the product and reactant bands.

Equilibrium Polymerase-DNA Binding Experiments—The binding affinity of the DNA to the polymerase was evaluated with fluorescence anisotropy. The DNA (1 nM) consisted of the primer strand modified on the 5′-end with 6-carboxyfluorescein and the template strand containing dG. The fluorescence anisotropy was measured with 0–100 nM pol ν at 37 °C using a Tecan Safire 2 plate reader with half-volume 96-well plates. The excitation and emission wavelengths were 471 and 525 nm, respectively, with an emission bandwidth of 20 nm.

Data Analysis—The kinetic constants were fit using GraphPad Prism Version 6. Computer simulations were performed with DynaFit Version 4 (BioKin Ltd.) (33).

Results

Purification and Concentration of pol ν—The His tag pol ν was purified with an imidazole gradient on an nickel-nitrilotriacetic acid column. From a 2-liter incubation, we obtained 2 ml of 990 nM protein. The active site concentration of pol ν was determined by measuring the burst amplitude of a reaction containing an excess of DNA and a saturating concentration of dNTP. As shown in Fig. 2, the reaction could be fit to Equation 1,

$$P = A(1 - e^{-k_f t}) + k_s t \qquad \text{(Eq. 1)}$$

where P is the concentration of the products; A is the burst amplitude; k_f is the rate constant of the fast phase, and k_s the steady-state rate constant. The burst amplitude of 6 ± 2 nM agreed with the protein concentration of 6.6 nM determined spectrophotometrically. The burst rate constant was >100 s^{-1} indicating that the polymerase has high catalytic activity.

Steady-state Incorporation of dNTPs Opposite dG—The Michaelis-Menten kinetic parameters determined with pol ν and the P15/T24 DNA substrate are shown in Table 2. The DNA sequence was chosen because we previously used this sequence to examine the reactivity of KF (32, 34–37). dCTP was incorporated opposite dG with k_{cat}/K_m values 5-fold
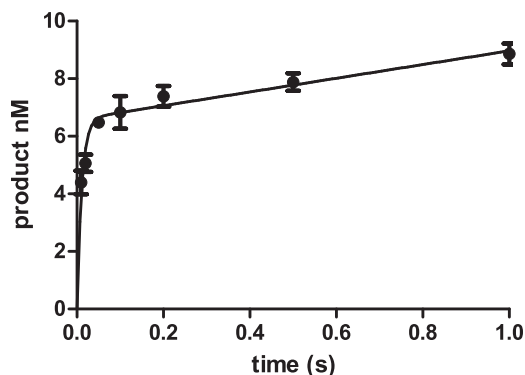

FIGURE 2. **Determination of pol ν concentration.** Reaction of 6.6 nM pol ν with 50 nM DNA and 500 μM dCTP. The data points are the mean ± S.D. of three experiments. The line is the best fit to Equation 1 with $A = 6.0 \pm 0.2$ nM, $k_f = 115 \pm 20$ s^{-1}, and $k_s = 3.9 \pm 0.5$ nM s^{-1}.

greater than dTTP. The purine triphosphates were incorporated about 10-fold less readily. The differences in k_{cat}/K_m values are driven by both the k_{cat} and K_m parameters. These numbers are consistent with the reports that pol ν is a low fidelity enzyme that is especially poor at discrimination against the incorporation of dT opposite dG in select sequences.

Pre-steady-state Incorporation of dNTPs—Steady-state kinetic analysis does not provide insights into intermediates in the reaction pathway of enzyme-catalyzed reactions. This is especially true of DNA polymerases because under conditions in which the DNA is in excess over the polymerase, the rate-limiting step is the dissociation of the DNA from the polymerase. Thus, to more fully explore the mechanisms by which pol ν catalyzes DNA replication, we performed pre-steady-state kinetic experiments. We carried out single-turnover reactions by preincubating 15 nM DNA with 150 nM polymerase and initiating the reaction by the addition of dNTP and 5 mM MgCl$_2$. The resulting time courses at different dNTP concentrations are shown in Fig. 3. The incorporation of dCTP (Fig. 3B) is much more rapid than the incorporation of incorrect dNTPs. For example, at a dNTP concentration of 100 μM, the half-life for the reaction of dCTP was 0.013 s, whereas that for incorrect dNTPs was ~6.5 s, a 500-fold dif-

TABLE 2
Steady-state parameters for the pol ν-catalyzed insertion opposite dG

Reactions contained 0.5 nM polymerase and a DNA concentration of 50 nM. Parameters are the mean of three experiments ± S.D. The error for f_{inc} was determined by propagation of errors.

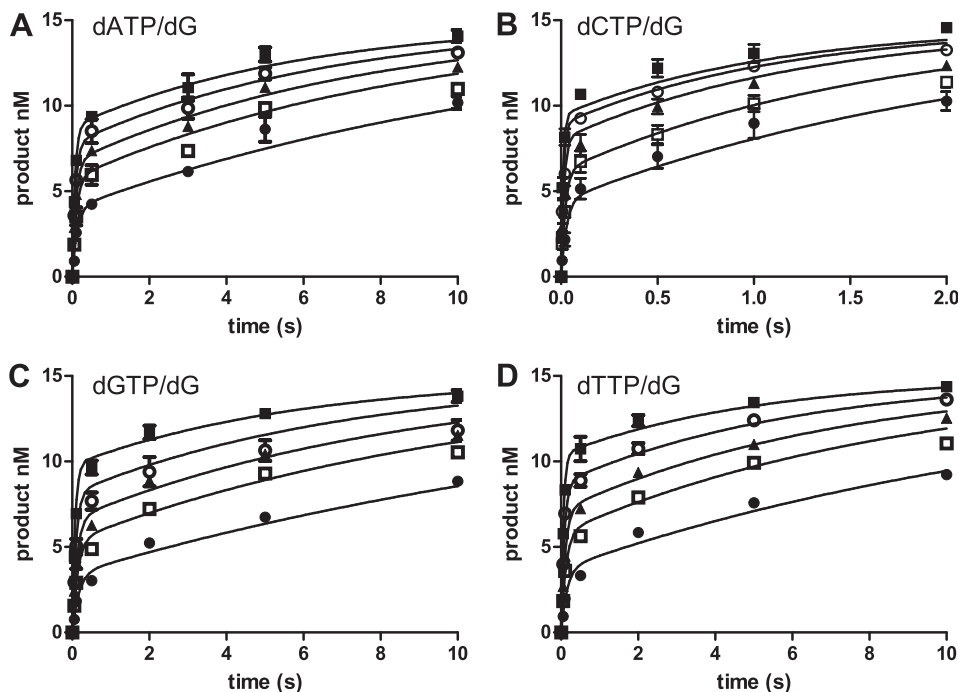| dNTP	k_{cat}	K_m	k_{cat}/K_m	f_{inc}
	s^{-1}	μM	s^{-1} M^{-1}	
dATP	0.0012 ± 0.0001	300 ± 56	42 ± 3	0.021 ± 0.005
dCTP	0.020 ± 0.002	11 ± 3	1950 ± 420	1
dGTP	0.0088 ± 0.0012	146 ± 49	63 ± 12	0.033 ± 0.009
dTTP	0.0085 ± 0.0005	24 ± 1	350 ± 20	0.18 ± 0.04

FIGURE 3. **Time course for the pol ν-catalyzed incorporation of dATP (A), dCTP (B), dGTP (C), and dTTP (D) opposite dG.** The pol ν concentration was 150 nM, and the DNA concentration was 15 nM. The dNTP concentrations were 5 (●), 10 (□), 25 (▲), 50 (○), and 100 (■) μM for dCTP and 100 (●), 200 (□), 300 (▲), 500 (○), and 1000 (■) μM for the other dNTPs. The data points are the mean of three experiments with standard deviations. The *lines* are computer simulation with the parameters in Table 5 for *A* and *B*. For *C* and *D*, the *lines* are based upon the parameters of dATP with the following changes: *C*, K_d for dGTP = 1.5 mM; $k_3 = 24$ s^{-1}; $k_{-3} = 10$ s^{-1}; $k_5 = 0.46$ s^{-1}; and *D*, K_d for dTTP = 2 mM; $k_3 = 37$ s^{-1}; $k_{-3} = 11$ s^{-1}; and $k_5 = 0.51$ s^{-1}.
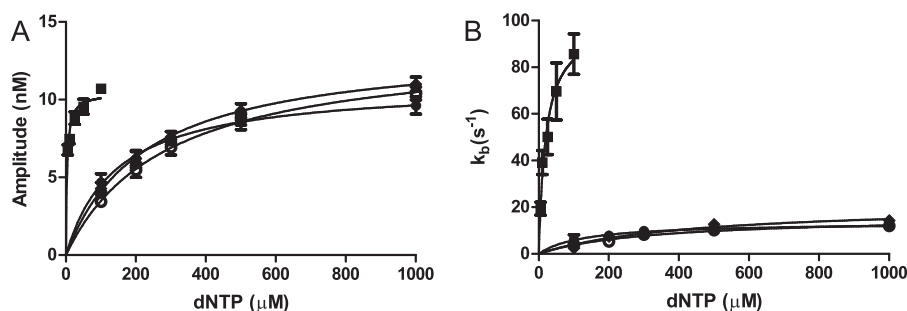
FIGURE 4. **Dependence of the amplitude (*A*) and burst rate constant (*B*) on the concentration of the dATP (■), dCTP (●), dGTP (○), and dTTP (♦) during the insertion opposite dG.** The data points are the mean ± S.D. of three experiments. The *solid line* is the best fit to Equation 2.

TABLE 3

Pre-steady-state kinetic parameters

Reactions contained 150 nM pol ν and 15 nM DNA. Parameters are the mean of three experiments ± S.D.

	A_{max}	K	k_{pol}	K_d^{app} for dNTP	k_s
	nM	*μM*	*s^{-1}*	*μM*	*nM s^{-1}*
dATP	11 ± 2	143 ± 10	14 ± 1	130 ± 20	0.53 ± 0.05
dCTP	11 ± 1	4.0 ± 1	100 ± 8	20 ± 5	2.3 ± 0.2
dGTP	12 ± 1	200 ± 20	15 ± 2	340 ± 70	0.48 ± 0.05
dTTP	13 ± 1	180 ± 30	21 ± 4	470 ± 150	0.49 ± 0.06

ference. This discrimination differs from the relative k_{cat}/K_m ratios that range from 5 to 50. In these single-turnover reactions, we do not observed a preference for dTTP incorporation over dATP or dGTP.

The time courses exhibited biphasic kinetics in which a rapid reaction was followed by a slower reaction. The time courses were initially fit to Equation 1. The amplitude (*A*) and burst rate constant *k* were dependent on the dNTP concentrations, whereas the steady-state rate constant (k_s) was not. The resulting amplitudes and burst rate constants are plotted against dNTP concentration in Fig. 4. These values were fitted to a hyperbola (Equation 2) in which *V* is the value of the parameter at a specific [dNTP]. From these plots, we obtained the following: A_{max}, the maximum amplitude; K_A, the [dNTP] at 50% of A_{max}; k_{pol}, the maximum burst rate constant and the apparent dissociation constant of the dNTP, and K_d^{app} for dNTP. These parameters as well as the k_s from the initial fitting are presented in Table 3. The k_{pol} for the incorporation of the correct dCTP is 100 ± 8 s^{-1}. This value is comparable with the values obtained from KF and T7 pol (11, 18) and is very similar to the k_{pol} of 155 s^{-1} for KF(exo−) with the same DNA substrate (37). This value is larger than the k_{pol} found for the Y-family polymerases κ and ι but similar to that of pol η (30, 38, 39).

$$V = \frac{V_{max}[N]}{[N] + K}$$ (Eq. 2)

The k_{pol} values for the incorrect dNTPs were 5-fold lower, ranging from 14 to 22 s^{-1}. These values are much larger than those for KF and T7 pol (12, 18, 28, 37). The K_d^{app} value for dNTP was lower for the correct dCTP (4.3 μM) than for the incorrect dNTPs (140−290 μM) by a factor of 30−70. The apparent K_d^{app} values for dNTP for the correct and incorrect dNTPs are similar to those found for KF and T7 pol. The burst amplitude was also dependent on the dNTP concentration. The maximum amplitude (A_{max}) for all four dNTPs were similar, ranging from 10 to 13 nM. The K_A value is lower for the correct

dCTP (20 μM) that the incorrect dNTPs (140−440 μM). In summary, dCTP is favored over the incorrect dNTPs by a higher k_{pol}, and lower K_d^{app} for dNTP and K_A values. In contrast to the steady-state experiments, we do not observe a preference of dTTP over dATP and dGTP.

The dNTP concentration dependence on the burst amplitude was not observed for KF and T7 pol. In this respect, pol ν is unique in A-family polymerases and indicates a difference in mechanism. In subsequent experiments, we considered two possible mechanisms illustrated in Fig. 1, *A* and *B*, to explain the [dNTP]-dependent decrease in burst amplitude. Fig. 1*A* is the seven-step mechanism that has been found for KF and T7 pol. It consists of conformational changes prior to and after phosphodiester bond formation. This mechanism would produce a dNTP-dependent burst if step 5 was rate-limiting. The mechanism in Fig. 1*B* contains an inactive complex and would produce a decreased burst if the inactive complex is stable such that k_{-8} or k_{-9} values are slower than k_{pol}. The presence of inactive complexes has been observed with DNA adducts (40, 41) and with pol κ with correct base pairs (42).

pol ν is unique in its propensity to incorporate dT opposite dG in some sequences (1, 25, 26, 43). Our DNA sequence, which showed a preference for dTTP incorporation under steady-state conditions, did not show any preference under single-turnover conditions.

DNA Binding Affinity—The binding affinity of the DNA to pol ν was measured by two methods, fluorescence anisotropy and active site titration. The fluorescence intensity did not change when polymerase was added (data not shown), consistent with the assumption that the fluorescein does not interact with the polymerase and change the binding affinity. The increase in anisotropy was plotted against polymerase concentration in Fig. 5*A*. The data were fitted to Equation 2, in which *V* is the increase in anisotropy, and [*N*] is polymerase concentration. The K_d for DNA was determined to be 6.5 ± 1.8 nM.
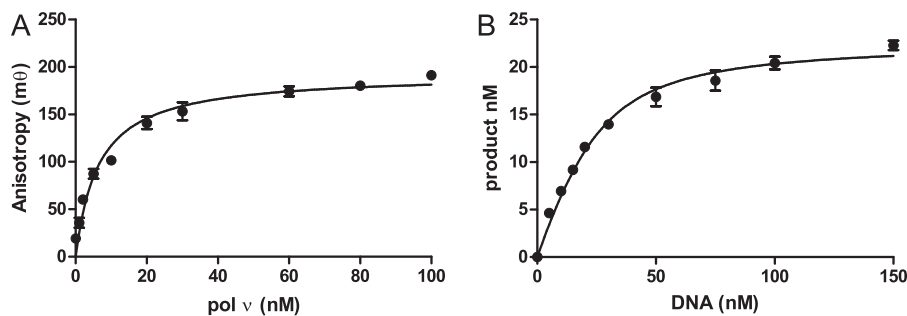
FIGURE 5. **DNA-pol ν affinity.** *A,* fluorescence anisotropy was determined with 1 nM DNA with 0–100 nM pol ν. The *line* is the best fit to Equation 2 resulting in a K_d for DNA of 6.5 ± 1.8 nM. *B,* active site titration was performed with 25 nM pol ν and 150 μM dCTP. The reaction was quenched at 1 s. The *line* is the best fit to Equation 3 result in a K_d for DNA of 9.2 ± 1.3 nM. The data points are the mean $\pm$ S.D. of three experiments.
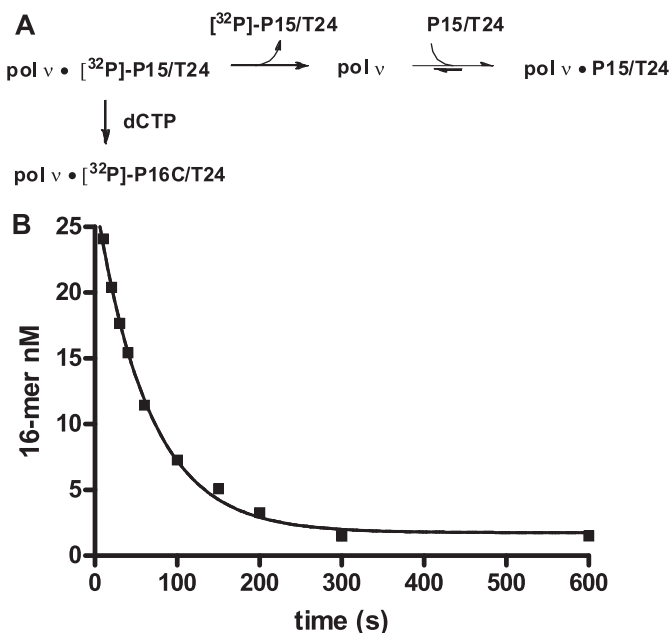

FIGURE 6. **Dissociation of DNA from pol ν.** *A,* description of the assay. *B,* preincubated ^{32}P-labeled P15/T24 (50 nM)/pol ν (25 nM) was mixed with 1 μM unlabeled P15/T24 for the indicated time, followed by addition of 200 μM dCTP. The reaction mixture was then allowed to incubate for an additional 15 s prior to being quenched by 0.3 M EDTA (pH 8.0). The data are the mean of three experiments $\pm$ S.D. The *solid line* is the best fit to Equation 4, with $k = 0.013 \pm 0.001$ s^{-1}.

The binding affinity was also measured by active site titration. In these experiments, pol ν was reacted with increasing amounts of DNA. The reaction was quenched after 100 ms, enough time for the burst phase of the reaction to be complete. The amount of product was plotted against DNA concentration, and the K_d for DNA and polymerase concentration (E) determined by fitting the data to Equation 3,

$$A = \frac{(E + D + K) - \sqrt{(E + D + K)^2 - 4ED}}{2} \quad \text{(Eq. 3)}$$

where A is the concentration of product; D is the DNA, and K is the K_d for DNA. By this procedure, the K_d for DNA was determined 9.2 ± 1.3 nM, consistent with the fluorescence anisotropy method. The enzyme concentration (E) was determined to be 22 ± 2 nM, consistent with the protein concentration determined in Fig. 1.

Dissociation Rate of the DNA—The dissociation rate of DNA and pol ν was determined by the procedure illustrated in Fig.

6A. pol ν (25 nM) was preincubated with ^{32}P-labeled P15/T24 (50 nM) in which the primer strand is 5′-^{32}P-labeled. The reaction was initiated by the addition of an excess of unlabeled trap DNA (P15/T24). The amount of ^{32}P-DNA still bound to the polymerase was assayed at various times by the addition of dCTP, which will react to form the 16-mer product. At time increases, the amount of 16-mer becomes less, as the ^{32}P-labeled P15/T24 substrate dissociates from the enzyme. The dissociation of the [^{32}P]DNA is essentially irreversible because of the large excess of unlabeled DNA. The data are presented in Fig. 6B. The *solid line* in Fig. 6B is the best fit to the single exponential in Equation 4,

$$P = Ae^{-kt} + C \quad \text{(Eq. 4)}$$

where P is the 16-mer concentration; A is the product concentration in the absence of the DNA trap; C is the product concentration at infinite time, and k the rate constant for the dissociation of the DNA from the protein, which was found to equal 0.013 ± 0.001 s^{-1}. This value, in combination with a K_d for DNA of 9.2 nM, leads to a DNA on rate constant of 1.4 μM^{-1} s^{-1}.

The mechanism in Fig. 1A predicts a first-order dissociation, whereas that in Fig. 1B would be biphasic, depending on the relative rate constants. Fig. 1B can account for the biphasic nature of the time course if conversion of the inactive complexes $E^X{\cdot}D_n$ and $E^X{\cdot}D_n{\cdot}dNTP$ to $E{\cdot}D_n$ and $E{\cdot}D_n{\cdot}dNTP$ were slow. Under this scenario the initial preincubation of enzyme and DNA would form both $E{\cdot}D_n$ and $E^X{\cdot}D_n$. Upon addition of dNTP, the fast phase would be the reaction of *ED* to product, whereas the slow phase would be the conversion of $E^X{\cdot}D_n$ to $E{\cdot}D_n$. However, the dissociation rate of 0.013 s^{-1} is slower than the slow phase in the reaction, and thus we cannot test this mechanism with this DNA dissociation mechanism.

Dissociation Rate of the dNTP—The off-rate of the dNTP is rapid for all polymerases examined thus far. To test whether this is also true for pol ν, we carried out trapping experiments described in Fig. 7. The ratio of the product of the trapped *versus* nontrap experiment should equal $k_{pol}/(k_{off} + k_{pol})$, in which k_{pol} is the forward rate to product formation, and k_{off} is the dNTP dissociation rate constant as shown in Fig. 1C. The nontrapped experiment was conducted as shown in Fig. 7A (●) in which the reaction of preincubated pol ν (60 nM), DNA (300 nM), and [α-^{32}P]dCTP (20 μM) was initiated by the addition of Mg^{2+}. The data in Fig. 7B was fit to the burst equation
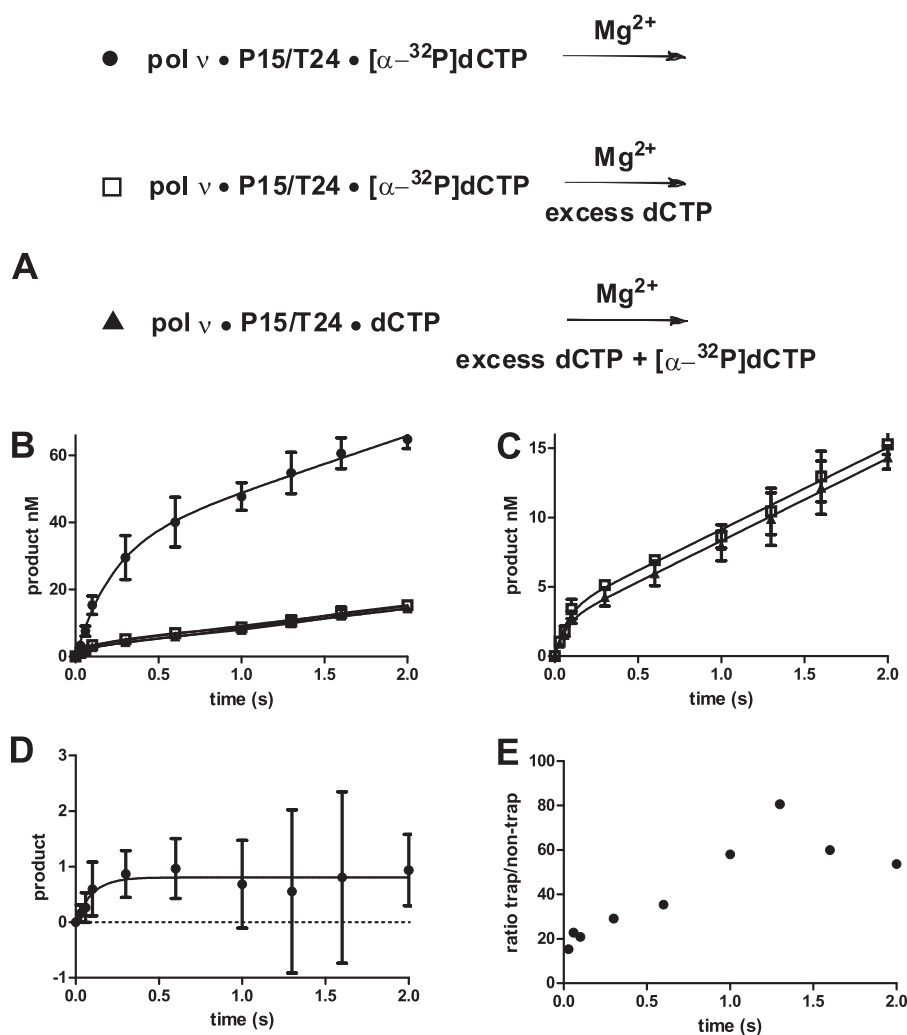
FIGURE 7. **Estimation of dNTP dissociation rate.** *A,* three assays used to estimate the dNTP off-rate constant. *B,* reaction between pol ν (60 nM), DNA (300 nM), and [α-^{32}P]dCTP (20 μM) with 5 mM Mg^{2+} (●). The *line* is the best fit to the burst equation with $A = 32 \pm 2$ nM, $k_f = 4.7 \pm 0.6$, and $k_s = 17 \pm 2$ nM s^{-1}. *B* and *C* (□), reaction between pol ν (60 nM), DNA (300 nM), and [α-^{32}P]dCTP (20 μM) with 6 mM Mg^{2+} and unlabeled 1 mM dCTP. The *line* is the best fit to the burst equation with $A = 3.2 \pm 0.3$ s^{-1}; $k_f = 13 \pm 3$; and $k_s = 5.9 \pm 0.3$ nM s^{-1}. *B* and *C* (▲), *line* is the best fit to the burst equation with 2.4 ± 0.3 nM; $k_f = 15 \pm 5$ s^{-1}; $k_s = 5.9 \pm 0.2$ nM s^{-1}. The data points are the mean ± 95% confidence intervals of four determinations. *D,* difference between the trap experiment (□) and control (▲) is plotted. The 95% confidence limits for the *error bars* were determined by error propagation (59), and the *line* is the best fit to a first-order equation. *E,* ratio of nontrapped (*A,* ●) to trapped (*D*) product formation.

to obtain an amplitude of 32 ± 2 nM and a burst rate constant of 4.6 ± 0.7 s^{-1}. The amount of product formed during the burst is dependent on the concentrations of both [pol ν·P15/T24·[α-^{32}P]dCTP] and [pol ν·P15/T24]. To determine the amount of product dependent on [pol ν·P15/T24·[α-^{32}P]dCTP], the trapped experiment (Fig. 7*A*, □) was performed by preincubating pol ν (60 nM), DNA (300 nM), and [α-^{32}P]dCTP (20 μM) and initiating the reaction with 1 mM dCTP and 6 mM Mg^{2+}. In this experiment, the [α-^{32}P]dCTP that dissociates will primarily be replaced by the unlabeled dCTP. This reaction was fit to the burst equation to obtain a reduced amplitude of 3.2 ± 0.3 nM. To determine the amount of product that is caused by the rebinding of [α-^{32}P]dCTP in the presence of 1 mM unlabeled dCTP, the experiment described by Fig. 7*A* (▲) was performed. In this protocol, pol ν (60 nM), DNA (300 nM), and dCTP (20 μM) were mixed with [α-^{32}P]dCTP (20 μM), dCTP (980 μM), and 6 mM Mg^{2+}. As shown in Fig. 7, *B* and *C* (▲), the reaction exhibited burst kinetics with an amplitude of 2.4 ± 0.3 nM.

The difference between the trapped experiment (□) and its control (▲) is shown in Fig. 7*D,* in which the *error bars* represent the 95% confidence intervals of the difference. Thus, the amplitude of the product resulting from the ternary complex is 0.8 nM *versus* the untrapped amplitude of 32 nM. This result is consistent with a rapid dissociation of dCTP from the ternary complex. The ratio of the products at the various time points is shown in Fig. 7*E.* During the first 0.25 s, the ratio is ~20. Because we found $k_{pol} = 100$ s^{-1}, the off-rate of the dNTP (k_{off}) is very fast, with a rate constant of ~2,000 s^{-1}. With a K_d^{app} for dNTP of 20 μM, we estimate the on-rate constant to be 10 μM^{-1} s^{-1}.

Pyrophosphorylation—The DNA polymerase-catalyzed reaction is reversible. Addition of pyrophosphate results in the successive removal of the terminal dNMP. The time course for pyrophosphorylation of the P16C/T24 DNA substrate at different concentrations of pyrophosphate is shown in Fig. 8*A.* The product in the *y* axis is the total of the 13-, 14-, and 15-mer that is formed during the reaction. The time courses can be fit to a
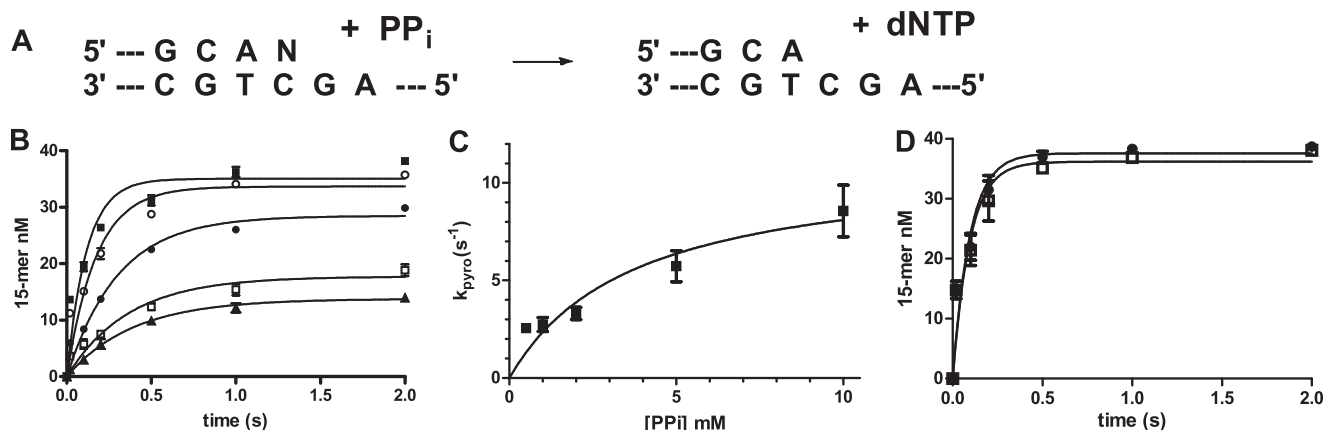
FIGURE 8. **Pyrophosphorylation.** *A,* pyrophosphorylation reaction. *B,* [PP$_i$]-dependent time course containing a matched terminal base pair (*n* = G). 40 nM DNA, 280 nM pol ν, and 5 mM MgCl$_2$ reacted with 0.5 (▲), 1 (□), 2 (♦), 5 (○), and 10 (■) mM pyrophosphate-MgCl$_2$. Data were fit to a first-order equation. *C,* phosphorylation rate constant is plotted against [PP$_i$] and fit to Equation l to obtain k_{pyro} = 11 ± 2 s^{-1}, and K_d for PP$_i$ = 3.7 ± 1.9 mM. *D,* pyrophosphorylation with a correct terminal base pair (P16C/T24, *n* = G, ●) and a terminal mispair (P16T/T24, *n* = A, □). The reaction contained 280 nM pol ν, 40 nM DNA, 10 mM PP$_i$, and 20 mM MgCl$_2$. Lines are best fit to first-order equation.
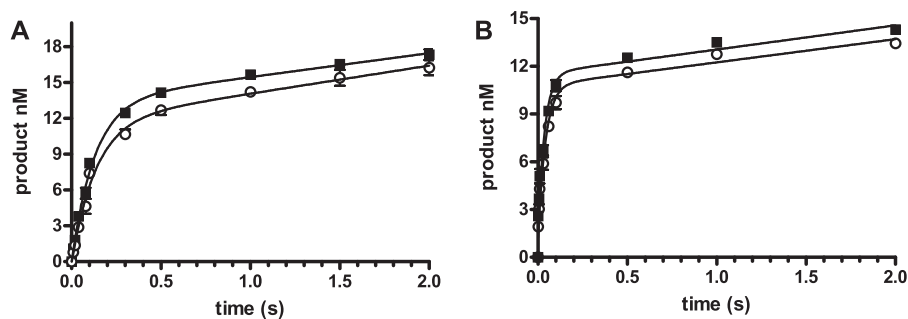

FIGURE 9. **Elemental sulfur effect.** DNA (20 nM), containing dG as the template base, was reacted with 40 nM pol ν with 5 μM dCTP (*A*), and 1 mM dATP (*B*). The data points are the mean ± S.D. of three experiments for dNTP (■) and dNTPαS (○). The *lines* are the best fit to Equation 1.

TABLE 4

Kinetic parameters for the elemental sulfur effect

Values are the mean ± S.D. of three experiments.

Substrate	A	k_f	k_s
	nM	*s^{-1}*	*nM s^{-1}*
dCTP	13.5 ± 0.3	7.8 ± 0.4	2.0 ± 0.2
dCTPαS	11.9 ± 0.4	7.4 ± 0.6	2.3 ± 0.2
dATP	10.0 ± 0.5	27 ± 4	1.5 ± 0.3
dATPαS	9.5 ± 0.4	24 ± 3	1.4 ± 0.3

first-order equation. The resulting rate constant can be fit to a hyperbola with a maximum rate of 11 ± 2 s^{-1}, and a K_d for PP$_i$ = 3.7 ± 1.9 mM (Fig. 8*B*). We also examined the rate of phosphorylation with a terminal mispair using P16T/T24. The reaction, containing 280 nM pol ν, 40 nM DNA, 10 mM PP$_i$, and 20 mM MgCl$_2$, shown in Fig. 8*C* demonstrates that the presence of a mispair does not affect pyrophosphorylation.

Elemental Sulfur Effect—The rate-limiting step was investigated using deoxynucleotide triphosphates in which a nonbridging oxygen on the α-phosphate is replaced by sulfur (dNTP(αS)). As shown in Fig. 9*A*, the reactions with 5 μM dCTP or dCTPαS exhibited similar kinetics. The reactions were fit to the burst equation with the parameters shown in Table 4. The kinetic parameters were virtually identical. This result is consistent with those for KF and T7 pol in which phosphodiester bond formation is rapid and such that the ~100-fold reduction in rate of this step did not affect the rate of phosphodiester bond formation. The elemental sulfur effect was also examined for

the misincorporation of dATP opposite dG. The time course profiles shown in Fig. 9*B* and parameters in Table 4 again demonstrate that the sulfur substitution had no effect on the reaction kinetics. This result suggests that phosphodiester bond formation is more rapid than the conformational change steps, a result very different from those obtained for KF and T7 pol, which had elemental effects of 65 for KF (12) and 13–37 for T7 pol (19) during incorrect base pair formation. These results indicate that phosphodiester bond formation is rapid for both correct and incorrect base pair formation.

Pulse-Chase Experiments—The pulse-chase experiment was performed to investigate the possibility of kinetic steps that precede and/or come after phosphodiester bond formation. In these experiments, pol ν/DNA was reacted with [α-^{32}P]dCTP for various times. Fig. 10*A* shows the 16-mer product formed after quenching with 1 N HCl (○) *versus* the pulse-chase (●) in which the reaction was quenched with 1 mM unlabeled dCTP for 30 s followed by 1 N HCl. The acid quenches all the enzyme-bound species, resulting in only the D_{n+1} species being recognized as product. When the reaction is chased with cold dCTP, an increase in product is observed, due to the forward reaction of D_n-containing species. These species cannot be $E·D_n$, because it will bind to unlabeled dCTP, or $E·D_n·$dNTP because the off-rate of the dNTP, (k_{-2}) is much greater than k_{pol}. Thus, these experiments support the existence of $E^*·D_n·$dNTP. In addition, the observation that the pulse-chase continuously
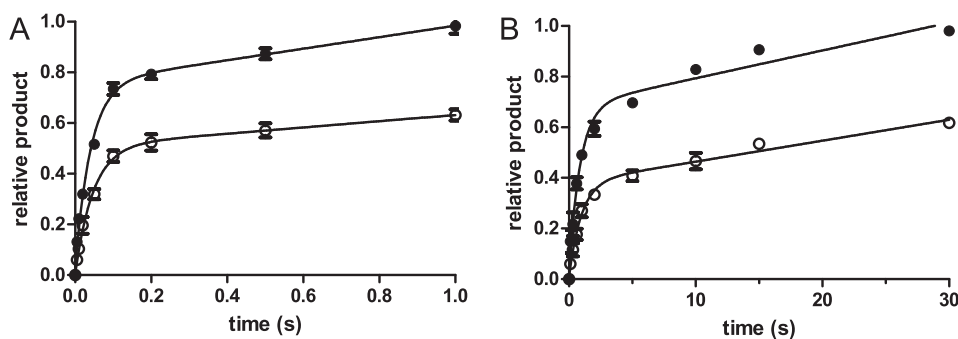
FIGURE 10. **Pulse-chase and pulse-quench experiments.** pol ν/DNA (50 nM each), containing dG as the template base, was mixed with 2.5 μM [α-^{32}P]dCTP (*left*) or [α-^{32}P]dATP (*right*) for various times. The reactions were quenched with 1 N HCl (○) or 1 mM dNTP for 30 s followed by 1 N HCl (●). The resulting acidic sample mixtures were extracted with 1 ml CHCl$_3$/*iso*-amyl alcohol (24:1) then neutralized with NaOH. The data points are the mean ± S.D. of four experiments. The data were fit to Equation 1.

forms a greater amount of product is consistent with a mechanism in which a kinetic roadblock follows the product formation step that was observed for KF (13). If k_5 was large, we would observe a transient increase in pulse-chased product as was observed with T7 pol (18). This observation supports the existence of $E^* \cdot D_{n+1} \cdot PP_i$. For dCTP, the amplitude of the pulse-quench is 69% that of the pulse-chase. Because step 5 is slow, we can estimate that $E^* \cdot D_{n+1} \cdot PP_i$ comprises the bulk of the D_{n+1} species. Thus, the ratio of ($E^* \cdot D_{n+1} \cdot PP_i$) to ($E^* \cdot D_n \cdot dNTP$) equals 0.69/0.31 and thus $K_4 = 2.2$. For dATP, the burst amplitude of the quench-chase experiment is 57% that of the pulse-chase experiment. By a similar analysis the $K_4 = 1.3$.

Computer Simulation—The kinetic scheme for the pol ν-catalyzed incorporation of dCTP opposite dG with the DNA substrate P15/T24 is consistent with the mechanism in Fig. 1*A* and the parameters in Table 5. For the simulation, several of the rate constants were set based upon the experiments described above. The rate constants for the association (1.4 μM^{-1} s^{-1}) and dissociation (0.013 s^{-1}) of the DNA and polymerase were set by the DNA affinity experiments in Fig. 5 and the DNA dissociation rate experiments in Fig. 6. These values were obtained for the P15/T24, and we assumed that the same values held for the product P16/T24. The off-rate constant for the dNTP (k_{-2}) was set to 2000 s^{-1} based upon the experiments shown in Fig. 7. The equilibrium constant for phosphodiester bond formation (k_4/k_{-4}) was set to 2.2 and 1.3 for dCTP and dATP, respectively, based upon the pulse-chase experiments in Fig. 10. The phosphodiester bond formation step is rapid, compared with step 3, because the incorporation of dCTP or dATP did not exhibit an elemental sulfur effect as shown in Fig. 9. The value for k_{-5} was set at 11 s^{-1} because this is the k_{pyro} obtained in Fig. 8. The K_d for PP$_i$ was set to be 3.7 mM based upon the experiments in Fig. 8. With these constants, the parameters k_{-2}, k_3, k_{-3}, and k_5 were fit by computer simulation. Initial estimates of k_{-2} was based upon the initial estimates for the K_d^{app} for dNTP parameters in Table 3. The initial estimates for k_3 and k_5 was based upon the maximal k_{pol} and k_s values from Table 3. Based upon these values, the parameters converged to those listed in Table 5. These calculated lines are shown in Fig. 3.

Discussion

pol ν catalyzes correct base pair formation with high efficiency, similar to KF and T7 pol. The k_{pol}, K_d for dNTP, and K_d

for DNA values are close to those found for T7 pol and KF (11, 18). The low fidelity of pol ν is due to its ability to rapidly catalyze mispair formation; the k_{pol} value decreased only 5-fold with a mispair. These results differs from those obtained with a 77-kDa construct of pol ν (pol ν-77) (26). The k_{pol} of pol ν-77 was found to be <1 s^{-1}, although we found a k_{pol} of 100 s^{-1}. This is also the construct that was recently crystallized (44). Our construct is that described by Takata *et al.* (24) in which a short C-terminal polyproline stretch is removed and FLAG and His tags were added. Interestingly, the k_{cat} and K_m values that we obtained are similar to those found for the pol ν-77 (44). We speculate that the excised N-terminal domain impacts the activity of the catalytic core.

pol ν catalyzes phosphodiester bond formation via the seven-step kinetic scheme that was formulated for the A-family polymerase KF (11–13, 27, 45, 46) and T7 pol (18, 19, 28, 47). The kinetic scheme for correct base pair formation by pol ν is very similar to that of KF and T7 pol, in that phosphodiester bond formation is much faster than the surrounding conformational changes. Although the major aspects of the kinetic mechanism are similar between pol ν and KF and T7 pol, there are small differences. pol ν is more like KF, with a rate-limiting step after phosphodiester bond formation and an equilibrium constant for phosphodiester bond formation (K_4) of 2.3 for pol ν and 4 for KF. In contrast, the rate-limiting step for T7 pol is the conformational change preceding bond formation (step 3), whereas $K_4 = 0.5$. pol ν differs from KF and T7 pol in that $K_3 = 0.75$, although it is 10 for KF (11, 12) and 3 for T7 pol (18).

The major difference between pol ν and its higher fidelity cousins occurs during mispair formation. The conformational change preceding bond formation and the bond formation step significantly decrease in rate with KF and T7 pol. However, with pol ν, phosphodiester bond formation remains rapid, although K_4 decreases from 2.3 to 1.3. Small decreases are also associated with the conformational changes; k_3 decreased from 75 to 13 s^{-1}, and k_5 decreased from 2.1 to 0.3 s^{-1}. Another difference between Kf and T7 pol and pol ν is the relative roles that polymerization and dNTP binding play in fidelity. For KF and T7 pol, the >1000-fold reduction in k_{pol} has more of an effect on fidelity than a 10-fold increase in K_d for DNA. In contrast, the 22-fold increase in K_d for dNTP plays a larger role in fidelity than the 5–7-fold decrease in k_{pol}.

ASBMB

TABLE 5

DNA polymerase ν kinetic constants

The kinetic constants represent the best fit of the kinetic and equilibrium data. The parameters in italics were determined by the experiments outlined in the text and set as constants. The other parameters were fit by DynaFit Version 4 using the time course parameters in Fig. 3.

Step			Correct base pair formation		Incorrect base pair formation dA/dG
1	$E + D_n \rightleftharpoons E{\cdot}D_n$	k_1	*1.4 μM^{-1} s^{-1}*	$K_d = 9.8$ nM	
		k_{-1}	*0.013 s^{-1}*		
2	$E{\cdot}D_n + dNTP \rightleftharpoons E{\cdot}D_n{\cdot}dNTP$	k_2	93 μM^{-1} s^{-1}	$K_d = 22$ μM	$K_d^{dNTP} = 476$ μM
		k_{-2}	*2,000 s^{-1}*		
3	$E{\cdot}D_n{\cdot}dNTP \rightleftharpoons E^*{\cdot}D_n{\cdot}dNTP$	k_3	75 s^{-1}		13 s^{-1}
		k_{-3}	101 s^{-1}		13 s^{-1}
4	$E^*{\cdot}D_n{\cdot}dNTP \rightleftharpoons E^*{\cdot}D_{n+1}{\cdot}PP_i$	k_4	*10,000 s^{-1}*.	$K = 2.2$	$K = 1.3$
		k_{-4}	4500 s^{-1}		
5	$E^*{\cdot}D_{n+1}{\cdot}PP_i \rightleftharpoons E{\cdot}D_{n+1}{\cdot}PP_i$	k_5	2.1 s^{-1}		0.5 s^{-1}
		k_{-5}	*11 s^{-1}*		11 s^{-1}
6	$E{\cdot}D_{n+1}{\cdot}PP_i \rightleftharpoons E{\cdot}D_{n+1} + PP_i$	k_6	*370,000 s^{-1}*	$K_d = 3.7$ mM	
		k_{-6}	*0.1 μM^{-1} s^{-1}*		
7	$E{\cdot}D_{n+1} \rightleftharpoons E + D_{n+1}$	k_7	*0.013 s^{-1}*	$K_d = 9.8$ nM	
		k_{-7}	*1.4 μM^{-1} s^{-1}*		

pol ν is more like pol η than pol κ. pol η catalyzes phosphodiester bond formation very rapidly, with k_{pol} values reported from 50 to 190 s^{-1} (48, 49). The elemental sulfur effect is small for both correct (1.6) and incorrect (2.5) base pair formation (48) indicating that the conformational changes are the primary rate-limiting steps. Thus, the low fidelity of pol η is due to a high rate of mispair formation. In contrast, k_{pol} for pol κ is lower, less than 10 s^{-1} (39, 50). The low fidelity is due to decreased correct base pair formation, rather than increased mispair formation. A similarity between pol κ and ν is the decreased burst amplitudes observed for correct base pair formation. However, the mechanisms that cause the decreased burst are different. pol κ forms a stable inactive complex that is kinetically detected by a biphasic dissociation of the DNA from the polymerase. With pol ν, we were not able to detect such a species. We have concluded that the decreased burst amplitude is due to $K_3 < 1$ and a rate-limiting step 5.

The high catalytic activity of pol ν is easy to rationalize based upon its sequence and structural similarities with KF, T7 pol, Taq pol, and BF. Simple homology modeling of the pol ν structure on those of BF, T7, and Taq pol shows that pol ν could potentially have identical interactions with the DNA. The recent pol ν crystal structure shows the active site structure of pol ν is very similar to that of the high fidelity A-family polymerases (44). Similarities include the binding surface between the polymerase and the DNA, with tight contact with minor groove and less contact with the major groove of the DNA. The amino acid residues that contact the terminal base pair and nascent base pair are totally conserved, as are the acidic residues that bind the critical Mg^{2+} ions. Thus, the positioning of

the nucleophilic 3′-hydroxyl on the DNA and the triphosphate is optimal for high catalytic activity.

Based upon the structural similarities between pol ν and KF, T7 pol, Taq pol, and BF, the low fidelity of pol ν is more difficult to understand. High fidelity polymerases are able to insert the correct *versus* incorrect dNTP at a ratio of 10^4–10^6 to 1. A current hypothesis is that polymerases amplify the differences in energy and structure of correct *versus* mispairs to both enhance the rate of correct base pair formation and decrease the rate of mispair formation (51–53). During T7 pol-catalyzed mispair formation, the energy of the $E^*{\cdot}D{\cdot}dNTP$ complex containing the incorrect dNTP is much higher in energy than that for the correct dNTP. In addition, the energy of the phosphoryl-transfer transition state is also drastically increased (28, 54). Thus, incorrect dNTPs are rejected in a two-step process because of the high energies of the closed complex as well as the transition state. The structures of these complexes as well as the interactions that account for the differences in energies between correct and incorrect base pairs are key for elucidating the mechanisms that polymerases use for base discrimination.

Two potential mechanisms by which mispairs are formed include the following: 1) non-Watson-Crick geometry base pairs such as wobble or Hoogsteen base pairs, and 2) Watson-Crick geometry base pairs that occur via the minor tautomers or ionized bases. Evidence for both mechanisms is found in crystallography experiments. Johnson and Beese (17) captured mispaired oligodeoxynucleotide substrates bound to BF. These structures show that BF readily discriminates against mismatches, binding them in inactive conformations. Crystal structures also indicate that a dT/dG mispair forms first as a

wobble base pair in the active site of a partially open BF (55), followed by formation of a closed polymerase conformation in which the base pair adopts Watson-Crick geometry in which one of the bases isomerizes to its minor tautomer (56). In contrast, structures of mispairs with bacteriophage *RB69* DNA polymerase, a high fidelity B-family polymerase, show the binding of mispairs in non-Watson-Crick geometry (57).

Therefore, pol ν can potentially accelerate mispair formation in two ways as follows: 1) by providing interactions that stabilize the Watson-Crick geometry of mispairs via minor tautomers or ionized bases, and/or 2) relaxing the geometric selection in the active site so that non-Watson-Crick structures can bind, although the polymerase adopts the catalytically active closed configuration. pol ν has several minor structural differences with KF, T7 pol, Taq pol, and BF. These include substitutions of two amino acid residues that contact the DNA as well as amino acid substitutions and insertions that are distally located throughout the polymerase domain. None of these changes lead to clear-cut mechanisms that explain why the incorporation of mispairs is not disfavored by pol ν. It is more likely that several of the differences contribute to the overall reactivity.

Although most of the amino acid substitutions are located distally from the DNA, two, Lys-679 and Glu-675, are located in the major groove of the DNA near the nascent base pair (44). Lys-679 is a Thr in T7 and Taq pol, and an Ala in KF and BF, and Glu-675 is an Arg in KF, T7 pol, Taq pol, and BF. The K679A mutation demonstrated that the lysine contributes to the propensity to incorporate dT opposite dG (43, 44). The lysine or glutamate may contribute to the stability of mispairs by forming hydrogen bonds to the non-Watson-Crick base pairs. Alternatively, they could provide electrostatic stabilization to minor tautomers or ionized base pairs (56, 58).

pol ν appears to have all the necessary amino acid residues to select for Watson-Crick base pairs. The residues that form the steric constraints for the nascent base pair and interact with the minor groove of the DNA are conserved (1, 44). Based upon the structural similarities, one would expect that a mispaired nascent base pair would lead to structural changes in the binding site that are transmitted to the active site so that catalysis does not occur. However, this does not happen with pol ν, suggesting that the connection between the Watson-Crick checking changes in the catalytic site are disrupted with pol ν. The many differences between pol ν and the high fidelity A-family polymerases that are located away from the DNA can lessen the fidelity by promoting a more flexible protein that is not as responsive to mispairs. For instance, although Arg-571 and Gln-769 are in position to make minor groove interactions at or adjacent to the nascent base pair, further away from the active site, the hydrogen bonding network between amino acid residues, water molecules, and the minor groove of the DNA are not observed in pol ν. These differences may compromise the ability of pol ν from adopting unreactive conformations that prevent the formation of mispairs.

A unique finding by Lee *et al.* (44) is the unusual open state in which the O and Ob helices exclude the template from the active site while allowing the dNTP to bind. In our kinetic model, the dNTP-bound state could potentially correspond to $E \cdot D_n \cdot dNTP$ in Fig. 1*A*. This model would predict that the binding affinity of the dNTP would not be dependent on the template base. We find, however, the binding affinity of the correct dNTP is 20-fold larger than the incorrect dNTPs, values similar to other A-family polymerases (37). Thus, we do not kinetically detect the unusual open conformation observed in the crystal structure. This conformation can be a transiently formed structure that exists during the binding of the dNTP to the DNA and polymerase that was stabilized by the crystallization procedure.

In summary, we have found that pol ν forms both correct and incorrect base pairs with high catalytic efficiency. Despite having all the amino acid residues that function to probe for Watson-Crick geometry in the high fidelity A-family polymerases, pol ν does not prevent mispair formation. Further studies with pol ν may reveal how interactions in the binding site of the polymerase are transmitted to the active site to modulate polymerase activity.

References

1. Marini, F., Kim, N., Schuffert, A., and Wood, R. D. (2003) POLN, a nuclear polA-family DNA polymerase homologous to the DNA cross-link sensitivity protein Mus308. *J. Biol. Chem.* **278,** 32014–32019
2. Prakash, S., Johnson, R. E., and Prakash, L. (2005) Eukaryotic translesion synthesis DNA polymerases: specificity of structure and function. *Annu. Rev. Biochem.* **74,** 317–353
3. Waters, L. S., Minesinger, B. K., Wiltrout, M. E., D'Souza, S., Woodruff, R. V., and Walker, G. C. (2009) Eukaryotic translesion polymerases and their roles and regulation in DNA damage tolerance. *Microbiol. Mol. Biol. Rev.* **73,** 134–154
4. Hubscher, U., Maga, G., and Spadari, S. (2002) Eukaryotic DNA polymerases. *Annu. Rev. Biochem.* **71,** 133–163
5. Boyd, J. B., Sakaguchi, K., and Harris, P. V. (1990) mus308 mutants of *Drosophila* exhibit hypersensitivity to DNA cross-linking agents and are defective in a deoxyribonuclease. *Genetics* **125,** 813–819
6. Pang, M., McConnell, M., and Fisher, P. A. (2005) The *Drosophila* mus308 gene product, implicated in tolerance of DNA interstrand cross-links, is a nuclear protein found in both ovaries and embryos. *DNA Repair* **4,** 971–982
7. Moldovan, G. L., Madhavan, M. V., Mirchandani, K. D., McCaffrey, R. M., Vinciguerra, P., and D'Andrea, A. D. (2010) DNA polymerase POLN participates in cross-link repair and homologous recombination. *Mol. Cell. Biol.* **30,** 1088–1096
8. Zietlow, L., Smith, L. A., Bessho, M., and Bessho, T. (2009) Evidence for the involvement of human DNA polymerase N in the repair of DNA interstrand cross-links. *Biochemistry* **48,** 11817–11824
9. Yamanaka, K., Minko, I. G., Takata, K., Kolbanovskiy, A., Kozekov, I. D., Wood, R. D., Rizzo, C. J., and Lloyd, R. S. (2010) Novel enzymatic function of DNA polymerase ν in translesion DNA synthesis past major groove DNA-peptide and DNA-DNA cross-links. *Chem. Res. Toxicol.* **23,** 689–695
10. Mizrahi, V., Henrie, R. N., Marlier, J. F., Johnson, K. A., and Benkovic, S. J. (1985) Rate-limiting steps in the DNA polymerase I reaction pathway. *Biochemistry* **24,** 4010–4018
11. Kuchta, R. D., Mizrahi, V., Benkovic, P. A., Johnson, K. A., and Benkovic, S. J. (1987) Kinetic mechanism of DNA polymerase I (Klenow). *Biochemistry* **26,** 8410–8417
12. Kuchta, R. D., Benkovic, P., and Benkovic, S. J. (1988) Kinetic mechanism

whereby DNA polymerase I (Klenow) replicates DNA with high fidelity. *Biochemistry* **27,** 6716–6725

13. Dahlberg, M. E., and Benkovic, S. J. (1991) Kinetic mechanism of DNA polymerase I (Klenow fragment): identification of a second conformational change and evaluation of the internal equilibrium constant. *Biochemistry* **30,** 4835–4843

14. Doublié, S., Tabor, S., Long, A. M., Richardson, C. C., and Ellenberger, T. (1998) Crystal structure of a bacteriophage T7 DNA replication complex at 2.2 Å resolution. *Nature* **391,** 251–258

15. Rothwell, P. J., Mitaksov, V., and Waksman, G. (2005) Motions of the fingers subdomain of Klentaq1 are fast and not rate limiting: implications for the molecular basis of fidelity in DNA polymerases. *Mol. Cell* **19,** 345–355

16. Kiefer, J. R., Mao, C., Braman, J. C., and Beese, L. S. (1998) Visualizing DNA replication in a catalytically active *Bacillus* DNA polymerase crystal. *Nature* **391,** 304–307

17. Johnson, S. J., and Beese, L. S. (2004) Structures of mismatch replication errors observed in a DNA polymerase. *Cell* **116,** 803–816

18. Patel, S. S., Wong, I., and Johnson, K. A. (1991) Pre-steady-state kinetic analysis of processive DNA replicative including complete characterization of an exonuclease-deficient mutant. *Biochemistry* **30,** 511–525

19. Wong, I., Patel, S. S., and Johnson, K. A. (1991) An induced-fit kinetic mechanism for DNA replication fidelity: direct measurement by single-turnover kinetics. *Biochemistry* **30,** 526–537

20. Lee, Y. S., Johnson, K. A., Molineux, I. J., and Yin, Y. W. (2010) A single mutation in human mitochondrial DNA polymerase pol γA affects both polymerization and proofreading activities of only the holoenzyme. *J. Biol. Chem.* **285,** 28105–28116

21. Longley, M. J., Nguyen, D., Kunkel, T. A., and Copeland, W. C. (2001) The fidelity of human DNA polymerase γ with and without exonucleolytic proofreading and the p55 accessory subunit. *J. Biol. Chem.* **276,** 38555–38562

22. Johnson, A. A., and Johnson, K. A. (2001) Fidelity of nucleotide incorporation by human mitochondrial DNA polymerase. *J. Biol. Chem.* **276,** 38090–38096

23. Graziewicz, M. A., Longley, M. J., and Copeland, W. C. (2006) DNA polymerase γ in mitochondrial DNA replication and repair. *Chem. Rev.* **106,** 383–405

24. Takata, K., Shimizu, T., Iwai, S., and Wood, R. D. (2006) Human DNA polymerase N (POLN) Is a low fidelity enzyme capable of error-free bypass of 5S-thymine glycol. *J. Biol. Chem.* **281,** 23445–23455

25. Arana, M. E., Takata, K., Garcia-Diaz, M., Wood, R. D., and Kunkel, T. A. (2007) A unique error signature for human DNA polymerase ν. *DNA Repair* **6,** 213–223

26. Arana, M. E., Potapova, O., Kunkel, T. A., and Joyce, C. M. (2011) Kinetic analysis of the unique error signature of human DNA polymerase ν. *Biochemistry* **50,** 10126–10135

27. Carroll, S. S., Cowart, M., and Benkovic, S. J. (1991) A mutant of DNA polymerase I (Klenow fragment) with reduced fidelity. *Biochemistry* **30,** 804–813

28. Tsai, Y. C., and Johnson, K. A. (2006) A new paradigm for DNA polymerase specificity. *Biochemistry* **45,** 9675–9687

29. Beckman, J. W., Wang, Q., and Guengerich, F. P. (2008) Kinetic analysis of correct nucleotide insertion by a Y-family DNA polymerase reveals conformational changes both prior to and following phosphodiester bond formation as detected by tryptophan fluorescence. *J. Biol. Chem.* **283,** 36711–36723

30. Zhao, L., Pence, M. G., Eoff, R. L., Yuan, S., Fercu, C. A., and Guengerich, F. P. (2014) Elucidation of kinetic mechanisms of human translesion DNA polymerase κ using tryptophan mutants. *FEBS J.* **281,** 4394–4410

31. Dunn, D. B., and Hall, R. H. (1986) in *Handbook of Biochemistry and Molecular Biology* (Fasman, G. D., ed) pp. 65–215, CRC Press, Inc., Boca Raton, FL

32. Meyer, A. S., Blandino, M., and Spratt, T. E. (2004) *E. coli* DNA polymerase I (Klenow fragment) uses a hydrogen bonding fork from Arg[668] to the primer terminus and incoming deoxynucleotide triphosphate to catalyze DNA replication. *J. Biol. Chem.* **279,** 33043–33046

33. Kuzmic, P. (2009) DynaFit–a software package for enzymology. *Methods Enzymol.* **467,** 247–280

34. Spratt, T. E. (1997) Enzyme-nucleotide interactions during DNA replication. *Biochemistry* **36,** 13292–13297

35. Spratt, T. E., and Levy, D. E. (1997) Structure of the hydrogen bonding complex of *O*6-methylguanine with cytosine and thymine during DNA replication. *Nucleic Acids Res.* **25,** 3354–3361

36. Spratt, T. E. (2001) Identification of hydrogen bonds between *Escherichia coli* DNA polymerase I (Klenow fragment) and the minor groove of DNA by amino acid substitution of the polymerase and atomic substitution of the DNA. *Biochemistry* **40,** 2647–2652

37. McCain, M. D., Meyer, A. S., Schultz, S. S., Glekas, A., and Spratt, T. E. (2005) Fidelity of mispair formation and mispair extension is dependent on the interaction between the minor groove of the primer terminus and Arg668 of DNA polymerase I of *E. coli*. *Biochemistry* **44,** 5647–5659

38. Sherrer, S. M., Sanman, L. E., Xia, C. X., Bolin, E. R., Malik, C. K., Efthimiopoulos, G., Basu, A. K., and Suo, Z. (2012) Kinetic analysis of the bypass of a bulky DNA lesion catalyzed by human Y-family DNA polymerases. *Chem. Res. Toxicol.* **25,** 730–740

39. Carlson, K. D., Johnson, R. E., Prakash, L., Prakash, S., and Washington, M. T. (2006) Human DNA polymerase κ forms nonproductive complexes with matched primer termini but not with mismatched primer termini. *Proc. Natl. Acad. Sci. U.S.A.* **103,** 15776–15781

40. Woodside, A. M., and Guengerich, F. P. (2002) Misincorporation and stalling at *O*6-methylguanine and *O*6-benzylguanine: evidence for inactive polymerase complexes. *Biochemistry* **41,** 1039–1050

41. Furge, L. L., and Guengerich, F. P. (1999) Explanation of pre-steady-state kinetics and decreased burst amplitude of HIV-1 reverse transcriptase at sites of modified DNA bases with an additional, non-productive enzyme-DNA-nucleotide complex. *Biochemistry* **38,** 4818–4825

42. Carlson, K. D., and Washington, M. T. (2005) Mechanism of efficient and accurate nucleotide incorporation opposite 7,8-dihydro-8-oxoguanine by *Saccharomyces cerevisiae* DNA polymerase η. *Mol. Cell. Biol.* **25,** 2169–2176

43. Takata, K., Arana, M. E., Seki, M., Kunkel, T. A., and Wood, R. D. (2010) Evolutionary conservation of residues in vertebrate DNA polymerase N conferring low fidelity and bypass activity. *Nucleic Acids Res.* **38,** 3233–3244

44. Lee, Y.-S., Gao, Y., and Yang, W. (2015) How a homolog of high-fidelity replicases conducts mutagenic DNA synthesis. *Nat. Struct. Mol. Biol.* **22,** 298–303

45. Eger, B. T., Kuchta, R. D., Carroll, S. S., Benkovic, P. A., Dahlberg, M. E., Joyce, C. M., and Benkovic, S. J. (1991) Mechanism of DNA replication fidelity for three mutants of DNA polymerase I: Klenow fragment KF(exo+), KF(polA5), and KF(exo−). *Biochemistry* **30,** 1441–1448

46. Eger, B. T., and Benkovic, S. J. (1992) Minimal kinetic mechanism for misincorporation by DNA polymerase I (Klenow fragment). *Biochemistry* **31,** 9227–9236

47. Donlin, M. J., and Johnson, K. A. (1994) Mutants affecting nucleotide recognition by T7 DNA polymerase. *Biochemistry* **33,** 14908–14917

48. Washington, M. T., Johnson, R. E., Prakash, L., and Prakash, S. (2003) The mechanism of nucleotide incorporation by human DNA polymerase η differs from that of the yeast enzyme. *Mol. Cell. Biol.* **23,** 8316–8322

49. Patra, A., Zhang, Q., Lei, L., Su, Y., Egli, M., and Guengerich, F. P. (2015) Structural and kinetic analysis of nucleoside triphosphate incorporation opposite an abasic site by human translesion DNA polymerase η. *J. Biol. Chem.* **290,** 8028–8038

50. Irimia, A., Eoff, R. L., Guengerich, F. P., and Egli, M. (2009) Structural and functional elucidation of the mechanism promoting error-prone synthesis by human DNA polymerase k opposite the 7,8-dihydro-8-oxo-2′-deoxyguanosine adduct. *J. Biol. Chem.* **284,** 22467–22480

51. Echols, H., and Goodman, M. F. (1991) Fidelity mechanisms in DNA replication. *Annu. Rev. Biochem.* **60,** 477–511

52. Kunkel, T. A. (2004) DNA replication fidelity. *J. Biol. Chem.* **279,** 16895–16898

53. Kool, E. T. (2002) Active site tightness and substrate fit in DNA replication. *Annu. Rev. Biochem.* **71,** 191–219

54. Joyce, C. M., and Benkovic, S. J. (2004) DNA polymerase fidelity: kinetics, structure, and checkpoints. *Biochemistry* **43,** 14317–14324

55. Wu, E. Y., and Beese, L. S. (2011) The structure of a high fidelity DNA polymerase bound to a mismatched nucleotide reveals an "Ajar" intermediate conformation in the nucleotide selection mechanism. *J. Biol. Chem.*

286, 19758–19767

56. Wang, W., Hellinga, H. W., and Beese, L. S. (2011) Structural evidence for the rare tautomer hypothesis of spontaneous mutagenesis. *Proc. Natl. Acad. Sci. U.S.A.* **108,** 17644–17648

57. Xia, S., Wang, J., and Konigsberg, W. H. (2013) DNA mismatch synthesis complexes provide insights into base selectivity of a B family DNA poly-

merase. *J. Am. Chem. Soc* **135,** 193–202

58. Hobza, P., and Sponer, J. (1999) Structure, energetics, and dynamics of the nucleic acid base pairs: nonempirical Ab initio calculations. *Chem. Rev.* **99,** 3247–3276

59. Bevington, P. R. (1969) *Data Reduction and Error Analysis for the Physical Sciences*, pp. 56–65, McGraw-Hill Inc., New York